



Article

Microwave Brightness Temperature (MBT) Background in Bayan Har Block, Qinghai-Tibet Plateau and Its Importance in Searching for Seismic MBT Anomalies

Yuan Qi ^{1,2}, Lixin Wu ^{1,2,*}, Yifan Ding ^{1,2}, Yingjia Liu ^{1,2}, Xiao Wang ^{1,2} and Wenfei Mao ^{1,2}

¹ School of Geosciences and Info-Physics, Central South University, Changsha 410083, China; qiyuan_rs@csu.edu.cn (Y.Q.); 215001016@csu.edu.cn (Y.D.); liuyingjia@csu.edu.cn (Y.L.); 215012193@csu.edu.cn (X.W.); maowenfei@csu.edu.cn (W.M.)

² Laboratory of Geo-Hazards Perception, Cognition and Predication, Central South University, Changsha 410083, China

* Correspondence: wulx66@csu.edu.cn

Abstract: The abnormal behaviors of microwave brightness temperature (MBT) before and after some strong inland earthquakes have been studied for more than 15 years, but the normal features of MBT background in the investigated regions still lack essential attention. This study focused on the extremely seismically active Bayan Har block on the Qinghai-Tibet Plateau in China, and revealed the spatiotemporal variations of monthly mean background and monthly standard deviation (STD) of MBT by using data of 10.65 and 89 GHz from AMSR-2 instrument. In terms of space, the results revealed that the MBT backgrounds at the two frequencies both basically exhibited a negative correlation with regional altitude but were more pronounced at high frequency. They also showed different response characteristics to the properties of soil and vegetation. In terms of time, the low-frequency background exhibited a complex month-to-month variation, with auxiliary data suggesting a joint contribution of surface soil moisture (SSM) and seasonal temperature; while the high-frequency background presented good agreement only with the variation in surface temperature. Meanwhile, the monthly STD of MBT was discovered being affected by SSM at the low-frequency and by snowfall events at the high-frequency. By employing MBT data of 10.65 GHz from AMSR-E and AMSR-2 sensors, the spatiotemporal evolutions of MBT anomalies before, during and after the Ms 7.1 Yushu earthquake on 13 April 2010 and the Ms 7.4 Maduo earthquake on 21 May 2021 were obtained referring to dynamic monthly mean background. A typical strip-shaped positive MBT anomaly just covering the Bayan Har block was found occurring prior to the two earthquakes, and the time series of average MBT anomaly inside the block was analyzed by using multiple datasets. The typical abnormal MBT strip was discriminated being independent of non-seismic factors and regarded as a possible precursor for both earthquakes. This research uncovered the normal features of MBT background and demonstrated the common characteristics of MBT anomalies preceding two strike-slip earthquakes inside the Bayan Har block. It has instructive significance for studying, understanding and searching for seismic MBT anomalies on Qinghai-Tibet Plateau.

Keywords: microwave brightness temperature; monthly mean background; seismic anomaly; Bayan Har block; Qinghai-Tibet Plateau; seismicity monitoring



Citation: Qi, Y.; Wu, L.; Ding, Y.; Liu, Y.; Wang, X.; Mao, W. Microwave Brightness Temperature (MBT) Background in Bayan Har Block, Qinghai-Tibet Plateau and Its Importance in Searching for Seismic MBT Anomalies. *Remote Sens.* **2022**, *14*, 534. <https://doi.org/10.3390/rs14030534>

Academic Editors: Fumio Yamazaki and Masashi Matsuoka

Received: 30 November 2021

Accepted: 21 January 2022

Published: 23 January 2022

Publisher's Note: MDPI stays neutral with regard to jurisdictional claims in published maps and institutional affiliations.



Copyright: © 2022 by the authors. Licensee MDPI, Basel, Switzerland. This article is an open access article distributed under the terms and conditions of the Creative Commons Attribution (CC BY) license (<https://creativecommons.org/licenses/by/4.0/>).

1. Introduction

Satellite remote sensing technology is playing an increasingly important role in monitoring abnormal phenomena and assessing damages caused by natural disasters, especially severe earthquakes (EQs) [1–14]. Passive microwave radiometers aboard satellites can provide abundant microwave observations of the Earth's surface and atmosphere due to their multi-band feature, dual polarisation and capability to penetrate the atmosphere and shallow surface [15,16]. They are the reason microwave brightness temperature (MBT)

data are eliciting increased attention. Passive microwave signals at low frequencies can reflect the thermal radiation and energy exchange on the Earth's surface. The dielectric properties of surface substances, which are particularly sensitive to water content [17], can dramatically affect the intensity of microwave radiation [16], especially at low frequencies. Meanwhile, MBT at high frequencies usually reflect more than the microwave radiation from the Earth's surface, and it is strongly affected by atmospheric water vapour and the presence of clouds [18,19]. In the natural state, the effects of geographical patterns and atmospheric environments can be reflected by the spatiotemporal features of MBT values.

MBT data from passive microwave radiometers have been utilised successfully to inverse surface soil moisture [20,21], land surface temperature [22,23], snow depth [24,25] and land surface emissivity [22,26,27]. More than a decade ago, researchers found that regional amplifications of MBT frequently occurred before and after several strong inland EQs [28–30]. Many methods and techniques have been proposed since then, and MBT data began to be adopted gradually in the study of seismic thermal anomalies. Through these efforts, numerous abnormal phenomena related to EQs, together with various features for different events, have been revealed [31–38]. Meanwhile, several experiments on remote sensing rock mechanics with microwave have been conducted to explore the mechanism of MBT anomalies in laboratory conditions [39–43]. These fundamental contributions have supported and promoted the research on seismic anomalies by using passive microwave satellite remote sensing.

Generally, a seismic thermal anomaly is regarded as the difference between what actually occurred in the shocking year and what was expected to happen based on a certain long-term trend. Accordingly, researchers subtract the background field value, which is constructed based on long-time series of historical data, from the data of the target seismic year to acquire abnormal residuals possibly associated with an EQ [6,33,35,44]. When the residual values are obtained, researchers usually focus on the spatiotemporal relationship of abnormal residuals with seismic activity then evaluate the potential correlations with the target EQ. Background fields based on historical MBT data are supposed to reflect spatial geographic patterns, landcover differences and even frequent meteorological disturbances in a study area. These features can represent the normal state of MBT in the study area under non-seismic conditions. Existing studies have suggested that seismic activity and EQ may generate an increment in microwave radiation in the process of EQ preparation, and this adds to the total amount of natural microwave radiation in the area. Prior knowledge of MBT in the usual state can be used as a basis to search for potential seismic MBT anomalies. However, only abnormal information was focused on in previous studies. Normal background information lacks essential attention.

In the past 30 years, the Bayan Har block on Qinghai–Tibet Plateau in China has been experiencing strong seismic activity [45], and the large EQs in mainland China ($M_s \geq 7.0$) all occurred inside or around the Bayan Har block. The northern boundary of the Bayan Har block is the east Kunlun fault, which is a huge, sinistral, strike-slip fault zone with a general strike in nearly EW direction [46]. On 21 May 2021 (UTC), a violent M_s 7.4 EQ occurred in Maduo, Qinghai Province, which is about 70 km south of the east Kunlun fault. The southern boundary of the Bayan Har block is the Ganzi–Yushu–Xianshuihe fault, which is also characterised by sinistral strike-slip and has been exhibiting extremely strong tectonic activity since the late Quaternary [45]. On 13 April 2010 (UTC), an extremely severe EQ with a magnitude of M_s 7.1 occurred in Yushu, Qinghai Province, which is located in the middle section of the Ganzi–Yushu–Xianshuihe fault. It caused massive life and property losses. The two strike-slip EQs were caused by the Indian plate pushing against the Eurasian plate and shared a similar seismic mechanism. Previous research has revealed that a thermal infrared (TIR) anomaly and enhanced abnormal MBT existed before the 2010 Yushu EQ [8,10,32], and another study showed that the outgoing longwave radiation (OLR) behaved unusually before the 2021 Maduo EQ [47]. Moreover, electromagnetic observations (electric or magnetic field) in the lithosphere and ionosphere indicated that electromagnetic anomalies occurred in different geospheres before the two EQs [48–50]. These phenomena

suggest that the two EQs caused electrical, magnetic and thermal anomalies in different forms, and further studies need to be conducted.

As exhibited in Figure 1a, the investigated region of this study is located at (29.5°N–36.5°N, 82°E–105°E), which covers the Bayan Har block entirely. The topography of the study area is characterized by low altitude in the east and high altitude in the west, rising from several hundred meters of elevation in the Sichuan Basin to several thousand meters in the hinterland of Qinghai-Tibet Plateau. In terms of the distribution of fault lines, the eastern segment of the Bayan Har block is densely faulted, indicating a complex fault system. Two strong strike-slip EQs with a magnitude greater than Ms 7.0, namely Yushu EQ on 13 April 2010 and Maduo EQ on 21 May 2021, occurred on its southern boundary and northern boundary, respectively. The epicentres of the two EQs are marked in red circles in Figure 1a. As shown in Figure 1b, grassland occupies most of the study area. Many plateau lakes are widely distributed in the western part of the study area, and the eastern part of the study area starts from the Longmenshan fault zone, which is covered with dense forests. The mainshock epicentres of the two EQs are both located in grassland areas, and the change features of landcover with season are relatively simple.

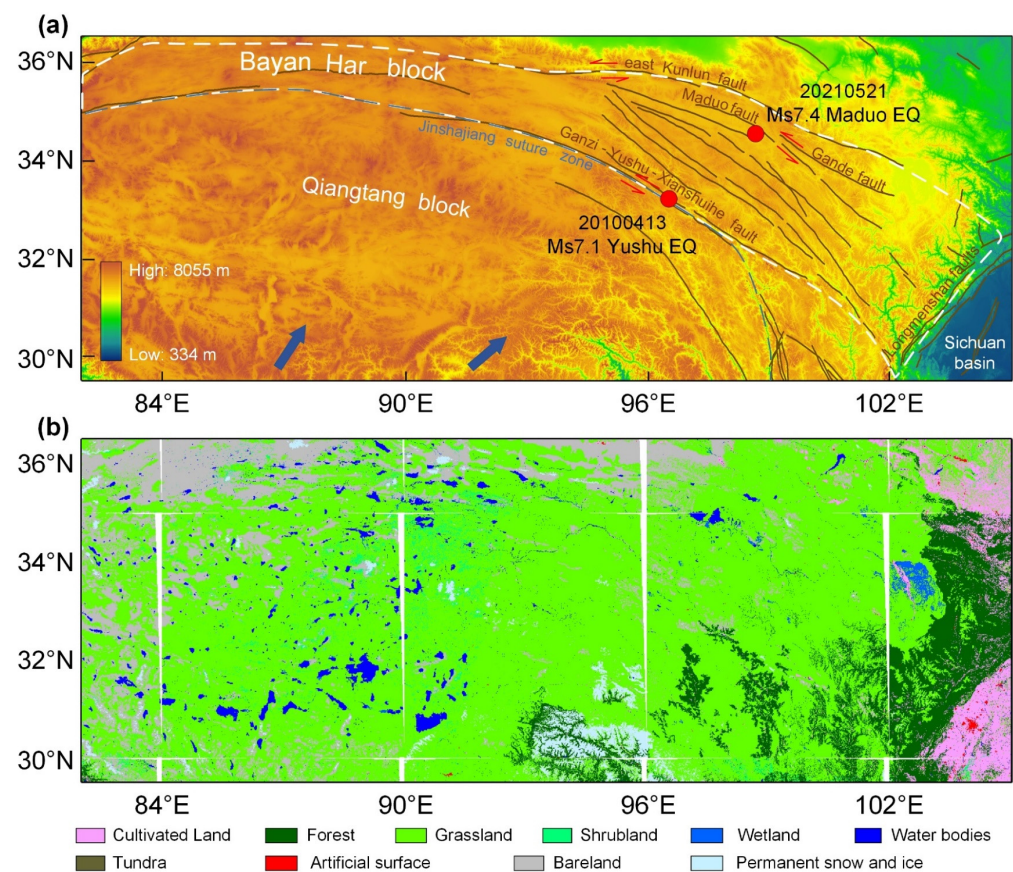


Figure 1. Distributions of surface elevation (a) and landcover (b) in the study area.

In this study, the monthly mean *MBT* background and its STD in the Bayan Har block were calculated using *MBT* data derived from the AMSR-2 instrument (June 2012 to August 2021). The spatiotemporal features were collaboratively analysed using auxiliary data, including skin temperature (SKT), 2 m air temperature (T2M), surface soil moisture (SSM) and snow depth. On the basis of the dynamic monthly mean background, *MBT* anomalies before and after the 2010 Yushu EQ and the 2021 Maduo EQ were revealed and analysed. A strip-shaped positive *MBT* anomaly covering exactly the Bayan Har block was found to have occurred prior to both EQs. Then, the time series of the average *MBT* anomalies inside the Bayan Har block was further analysed. Multiple auxiliary

datasets were also applied to exclude non-seismic disturbances to confirm the precursory relationship between the obtained typical MBT anomalies and the two strike-slip EQs.

2. Methods and Materials

2.1. MBT Background

The radiation signals received by a satellite microwave sensor mainly consist of two parts; one is from the Earth's surface, and the other is from the atmospheric medium (thick clouds and aerosols) along the transmission path. The proportion of the latter increases with microwave frequency. Literature has shown that the average of the time series of MBT data can eliminate the interference of random factors in the atmosphere and obtain the representative microwave radiation and emissivity of the ground surface with an optimal averaging window of 30 days [51]. Therefore, the monthly mean of MBT can be used to characterise the usual variation of microwave radiation in the study area over months. MBT data of the same month in all available years were adopted in the calculation in this study to obtain the monthly mean background, which represents the usual state for the same month in different years. The calculation can be described as follows:

$$MBT_{\tau} = \frac{\sum_{\psi=\alpha}^{\psi=\beta} \sum_{\lambda=1}^{\lambda=\kappa} MBT_{\psi,\tau,\lambda}}{\omega} \quad (1)$$

where ψ , τ and λ represent the year, month and day of MBT data used, respectively; κ is the total number of available days of month τ in year ψ . α and β refer to the start and end years of available MBT data in month τ , respectively, while ω stands for the total number of MBT data involved in the calculation. MBT_{τ} represents the monthly mean background of MBT in month τ in the study area.

2.2. MBT Data

All substances at a finite absolute temperature radiate electromagnetic energy [16]. When the spectral radiance of a ground object in a certain band is equal to that of a blackbody in the same band, the blackbody temperature is called the brightness temperature of the ground object. In other words, MBT represents the radiative capacity of an object in a particular direction in a microwave band. Since 1968, passive microwave sensors have been placed aboard many spacecraft systems, and the obtained global MBT observations have been widely used in the inversion of various parameters of the land surface and ocean [16]. The MBT data adopted in this study for the construction of the monthly mean MBT background was derived from the AMSR-2 instrument, which has been successfully providing microwave observations of the Earth for more than nine years. For the extraction of seismic MBT anomaly based on the monthly mean background, the selected MBT data should depend on the actual time of the studied EQ event. In a previous study, MBT data at H polarisation (H-pol) were determined to perform noticeably better in extracting seismic anomalies than data at V polarisation [14,35]. Thus, in the current study, MBT data at H-pol from AMSR-E and AMSR-2 instruments were selected to examine Yushu EQ in 2010 and Maduo EQ in 2021, respectively. The key parameters of the two sensors are shown in Table 1, and the information on the two EQs is shown in Table 2.

Table 1. Major performances of the AMSR-E and AMSR-2 instrument.

Parameter	AMSR-E						AMSR-2				
Platform	AQUA						GCOM-W1				
Available time	1 June 2002–4 October 2011						2 July 2021–present				
Frequency (GHz)	6.925	10.65	18.7	23.8	36.5	89.0	10.65	18.7	23.8	36.5	89.0
Polarization	H, V						H, V				
Spatial resolution (km)	50	50	25	25	15	5	50	25	25	15	5
IFOV (km × km)	43 × 75	29 × 51	16 × 27	18 × 32	8.2 × 14	3.7 × 6.5	42 × 24	22 × 14	26 × 15	12 × 7	5 × 3
NEΔT (K)	<0.34	<0.7	<0.7	<0.6	<0.7	<1.2	<0.7	<0.7	<0.6	<0.7	<1.2

Table 2. Information of the Yushu EQ and the Maduo EQ.

Information	Yushu Earthquake	Maduo Earthquake
Time (UTC)	13 April 2021	21 May 2021
Type	strike-slip	strike-slip
Magnitude (Ms)	7.1	7.4
Location	33.17°N, 96.55°E	34.65°N, 98.40°E
Hypocenter depth (km)	14	9

2.3. Auxiliary Data

Some synchronous satellite remote sensing data were adopted for auxiliary analysis in this work. SKT and T2M data were used to represent the physical temperature on the ground surface and that in surface air, respectively. The temperature and snow depth data were derived from ECMWF ERA5-Land reanalysis datasets, and their spatiotemporal resolution was 0.1° and 1 day, respectively. SSM and the precipitation data were from the NASA Global Land Data Assimilation (GLDAS) dataset (version 2.1) and had a spatiotemporal resolution of 0.25° and 3 h, respectively. GLDAS-2.1 uses satellite and ground-based observational data products instead of only depending on satellite microwave observations. Hence, it can be regarded as independent of the MBT data used in this research. The time span of the auxiliary data involved in the study was unified to that of MBT data.

3. Results and Analysis

3.1. Monthly Mean MBT Background and Its Standard Deviation (STD)

On the basis of all available data on the life cycle of the AMSR-2 sensor, the MBT data in the same month in different years were averaged to obtain the monthly mean MBT background. Figure 2 shows the variations of monthly mean MBT at 10.65 GHz (a) and 89.0 GHz (b) with H-pol in the Bayan Har block over 12 months of the year. Given that the altitude is high in the west and low in the east in the study area (see Figure 1a), the ground temperature and the monthly mean MBT backgrounds at the two frequencies were inversely low in the west and high in the east. In addition to the temperature effects of altitude change, the properties of surface soil and vegetation are also critical to MBT. With regard to the MBT background at 10.65 GHz, the values synthetically reflected the radiation from the shallow ground surface and volume scattering and the radiation from vegetation. The dominant vegetation type is forest in the eastern part of the study area, and it changes gradually to grassland. Thus, the vegetation density decreased as the altitude increased westward (Figure 1b), resulting in an increase in the contribution of bare soil and a decrease in the volume scattering of vegetation from east to west [52]. Therefore, the overall microwave emissivity and MBT at 10.65 GHz with H-pol showed a general trend of low in the west and high in the east.

With regard to the MBT background at 89 GHz, its intensity depends largely on the microwave contributions of the skin surface, vegetation canopy (if it exists) and atmosphere. The MBT values at high frequency were lower in winter and higher in summer than those at low frequency in a large western part of the study area. In winter, the ground surface of the western study area is mainly composed of snow, ice and frozen soil, and its dielectric constant exhibits little change with frequency. The inconsistency is due to the difference in penetration depth rather than in dielectric properties at the two frequencies. The temperature of the skin surface reflected by high-frequency MBT should be lower than the overall temperature of a certain thickness below the surface reflected by low-frequency MBT. In summer, low-frequency MBT reflects the radiation information of shallow soil with a certain water content, and high-frequency MBT reflects the additional effect of vegetation scattering [53]. Moreover, the dielectric of soil containing certain moisture decreases with frequency [16], which jointly contributes to the high MBT at high frequency in the western part of study area in summer. The high MBT at 89 GHz in the Longmenshan fault zone with dense vegetation is mainly due to vegetation scattering with increasing microwave

frequency, and that in the cultivated land in the eastern study area is primarily caused by the decrease in dielectric constant with increasing microwave frequency.

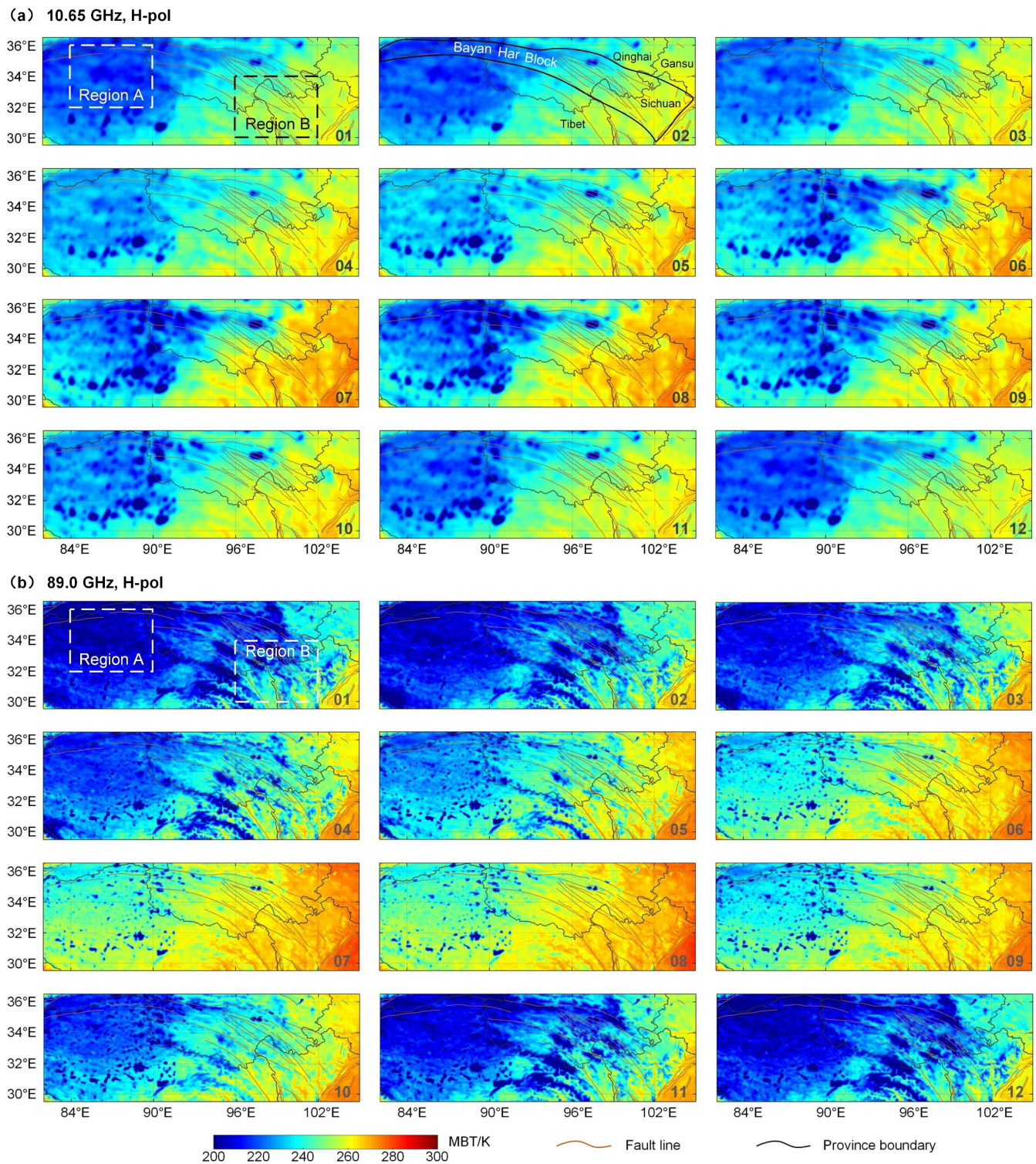


Figure 2. Monthly mean MBT background in the Bayan Har block and its surrounding area at 10.65 GHz (a) and 89.0 GHz (b) with H-pol (from January to December). The calculation was based on MBT data from the same month in different years.

The time-varying characteristics of the results at the two frequencies behaved differently. For the results at low frequency, the monthly mean MBT in the plateau area (high

altitude, such as region A) showed a complex trend of increasing two times then decreasing in a year, but the monthly mean MBT in the mountain area (relative low altitude, such as region B) showed only a trend of rising initially then declining, which is generally consistent with the atmospheric temperature variation throughout the year. The change cycles of the monthly mean MBT in the plateau area was as follows: it increased from January to May, decreased from May to August, increased again from August to October and decreased again from October to December. For the results at high frequency, the monthly mean MBT values in plateau and mountain areas are consistent with the variation in seasonal atmospheric temperature, that is, rising from spring to summer then declining from autumn to winter. The monthly varying curves of the dual-frequency MBT backgrounds in regions A and B are calculated and will be described in detail below.

In addition to the monthly mean MBT background, the STD of MBT per pixel was calculated using all available MBT data in the same month of different years. The purpose was to quantify the MBT difference in the same month but in different years. The results of STD reflect the local instability of MBT in the time dimension, which is also a manifestation of its inherent uncertainty in the state of nature. If the influencing factors of STD are clarified, it is beneficial for excluding disturbances of natural environment from the time series of MBT and then searching for disturbance information related to seismicity.

Figure 3 presents the variations of monthly STD of H-polarised MBT at 10.65 GHz (a) and 89.0 GHz (b) in the study area. With respect to the results at low frequency, the high values of STD are mainly presented as small blotchy areas from January to February and from October to December. These scattered areas correspond to the lakes in the plateau region. In addition, large areas with moderate STD values exist in the west-central part of the study area from March to September, and their scopes show a process of increasing first then decreasing later over the months. The values of STD at high frequency are generally higher than those at low frequency. The high values of STD are mainly concentrated in the east-central region of the study area, where Qinghai, Sichuan and Tibet meet, and appear locally in the southwest corner of the study area, which belongs to the Himalayan region, from January to May and from October to December. In the other months, the high values of high-frequency STD tend to occur in places with low elevations, especially in Sichuan Basin at the southeast corner of the study area. Similar to the low-frequency results, significant STD values were also found in the areas of plateau lakes in the high-frequency results but with better details due to the higher spatial resolution. This phenomenon may be caused by the dynamic changes in the areas of plateau lakes and the random effects of clouds over time.

3.2. Analysis of MBT Background and STD

Theoretically, microwave radiation emitted from the ground surface depends on its physical temperature and microwave emissivity; the latter is closely related to the surface dielectric property [16]. The monthly mean skin temperature (SKT) and 2 m air temperature (T2M) in the study area were calculated, and the contributions of temperature changes on the ground and in the air to dual-frequency MBT are analyzed. Generally, the spatial distribution features of T2M are consistent with that of SKT, but the values of T2M were slightly higher in winter and lower in summer. Given the spatial similarity of the results, they are demonstrated separately in Figure 4a (for SKT) and Appendix A Figure A1 (for T2M). Regions A, B and C in Figure 4 represent the plateau area, the mountainous area and the boundary area of the provinces in the study area, respectively. They were selected for comparative analysis of the spatiotemporal characteristics of the dual-frequency MBT background and STD, and other auxiliary data.

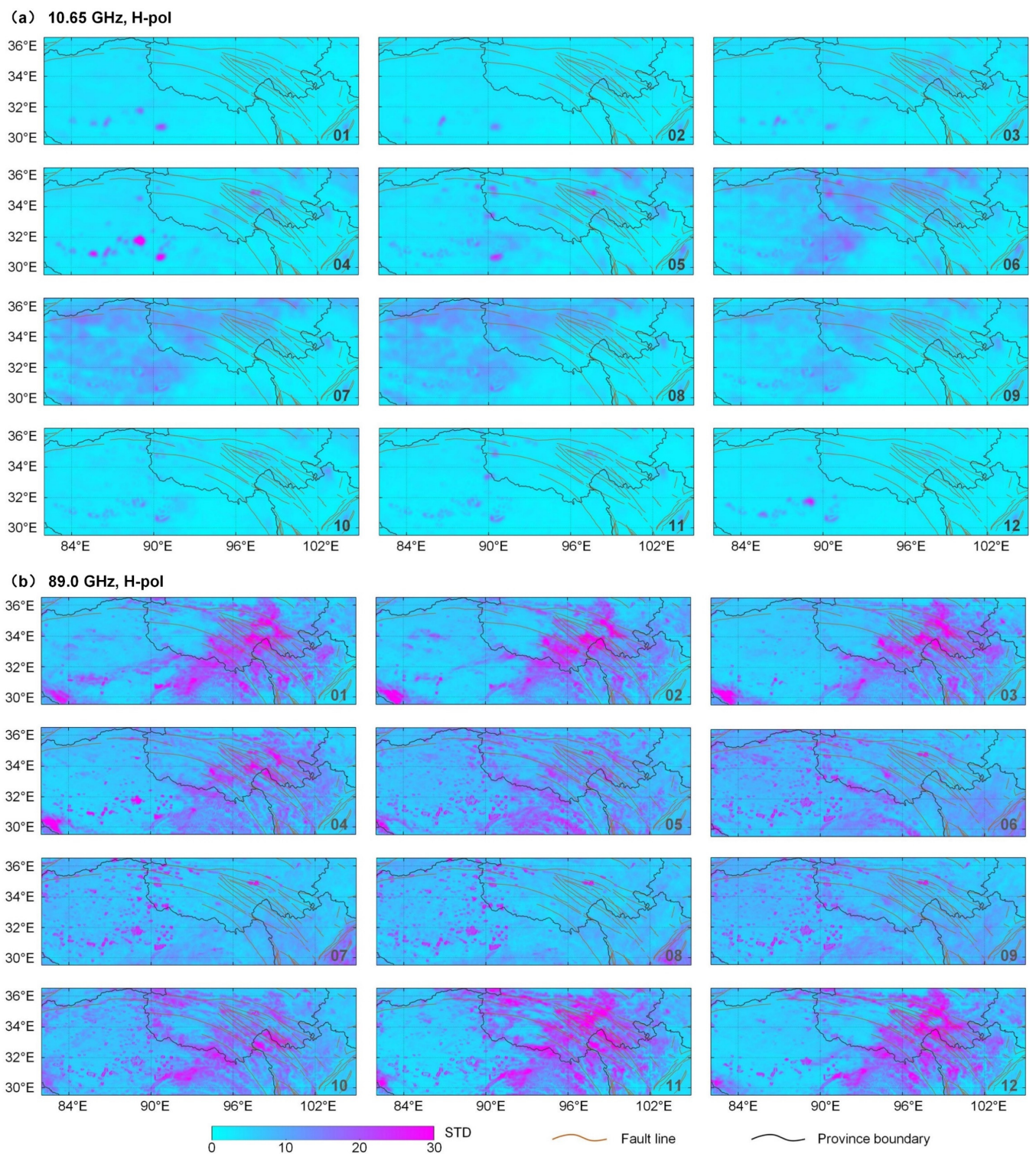


Figure 3. Monthly STD of MBT in the Bayan Har block and its surrounding area at 10.65 GHz (a) and 89.0 GHz (b) with H-pol (from January to December). The calculation was based on MBT data from the same month in different years.

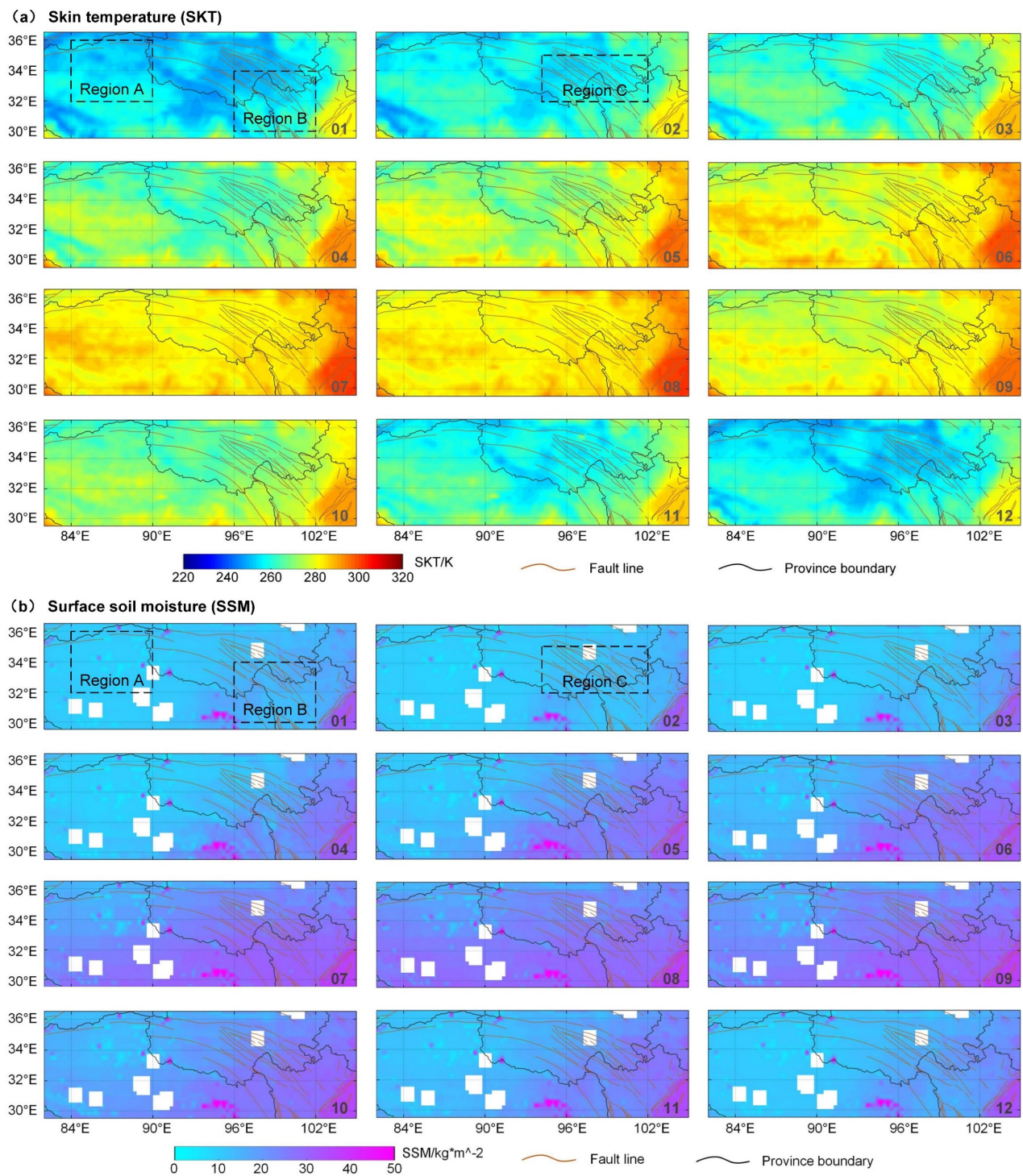


Figure 4. Monthly mean SKT (a) and SSM (b) in the study area. Region A, B and C represent the plateau area, the mountainous area and the boundary area of the provinces, respectively.

In terms of space, the values of SKT and T2M in the study area were relatively high in the east and low in the west, indicating that the spatial distributions of SKT and T2M were negatively correlated with altitude in the space pattern. Compared with the MBT background at low frequency (10.65 GHz), the spatial features of SKT and T2M were more consistent with those at high frequency (89 GHz), revealing that MBT at high frequency reflects the information of temperature change. In terms of time, the variations of SKT and T2M in the plateau area (such as region A) and the mountain area (such as region B) increased from January to July and decreased from July to December (Figure 5), which is

generally consistent with the temperature variation in a year. However, the variation of low-frequency MBT showed a high positive correlation with SKT in the low-altitude area (region B) but behaved much differently in the plateau area (region A), especially from May to September. This difference suggests that in addition to the contribution of atmospheric temperature to MBT, other decisive factors, such as emissivity variation, in the plateau area also exert effects during these months.

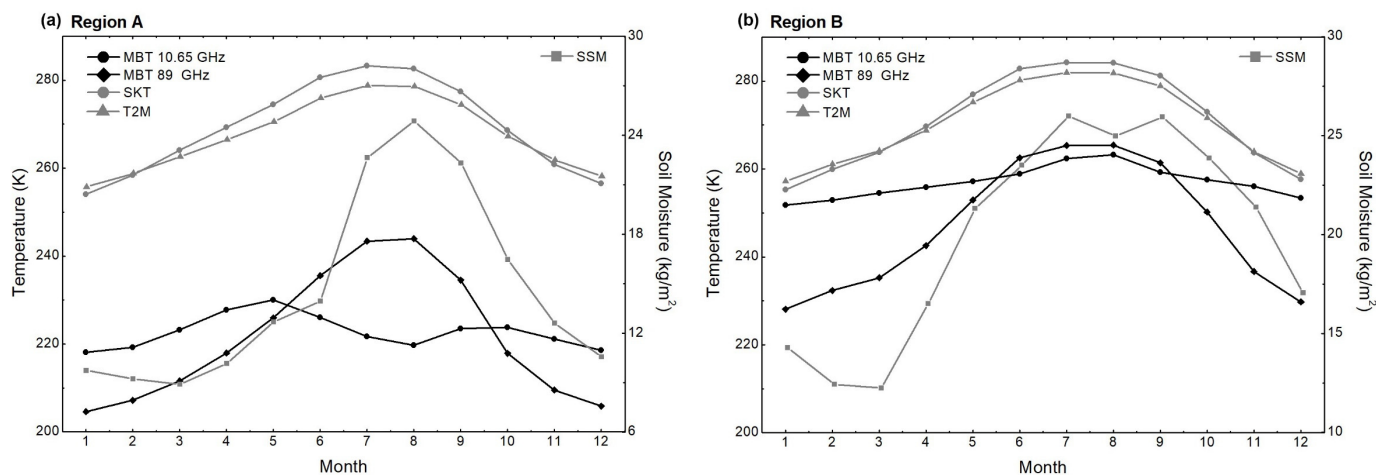


Figure 5. Variations of dual-frequency MBT, SKT, T2M and SSM in region A (a) and region B (b).

Microwave emissivity and dielectric constant are affected greatly by the water content of the surface medium [54]. Hence, the monthly mean SSM in the study area was calculated to analyse its potential influence on MBT through the dielectric constant. The result is shown in Figure 4b. Similar to the SKT result, the spatial distribution of SSM presented a characteristic of high in the east and low in the west and had a significant negative correlation with altitude. The high-SSM zone in the east of the study area extends gradually to the plateau area in the west month by month, and the zone's range and amplitude reach the peak in August then decrease until the end of the year. The monthly variations of SSM in regions A and B are shown in Figure 5. The average SSM in the two regions decrease from January to March and increase from March to May. This change in SSM is caused by the freezing–thawing process in the plateau region. The high value of SSM after May is attributed to the seasonal precipitation, which has an extremely weakening effect on MBT and leads to an evident decrease in MBT in the plateau area during summer.

Another notable finding is that the relatively low values of SKT and T2M in the east-central study area (region C) correspond well with the low value of monthly MBT and the high value of STD at high frequency (89 GHz) from November to March. This result indicates that the high values of STD at high frequency in these areas may be due to other particular factors that can lower the air temperature and exhibit some randomness over time. The same phenomenon was also observed in the Himalayan region in the southwest corner of the study area. Given the relatively high elevation of these areas and the low temperature in these months, we posit that the particular factor could be snowfall events. Therefore, the monthly mean snow depth in the study area was calculated, as shown in Figure 6. The quantitative results on snow depth and other multiple parameters in region C are shown in Appendix A Figure A2.

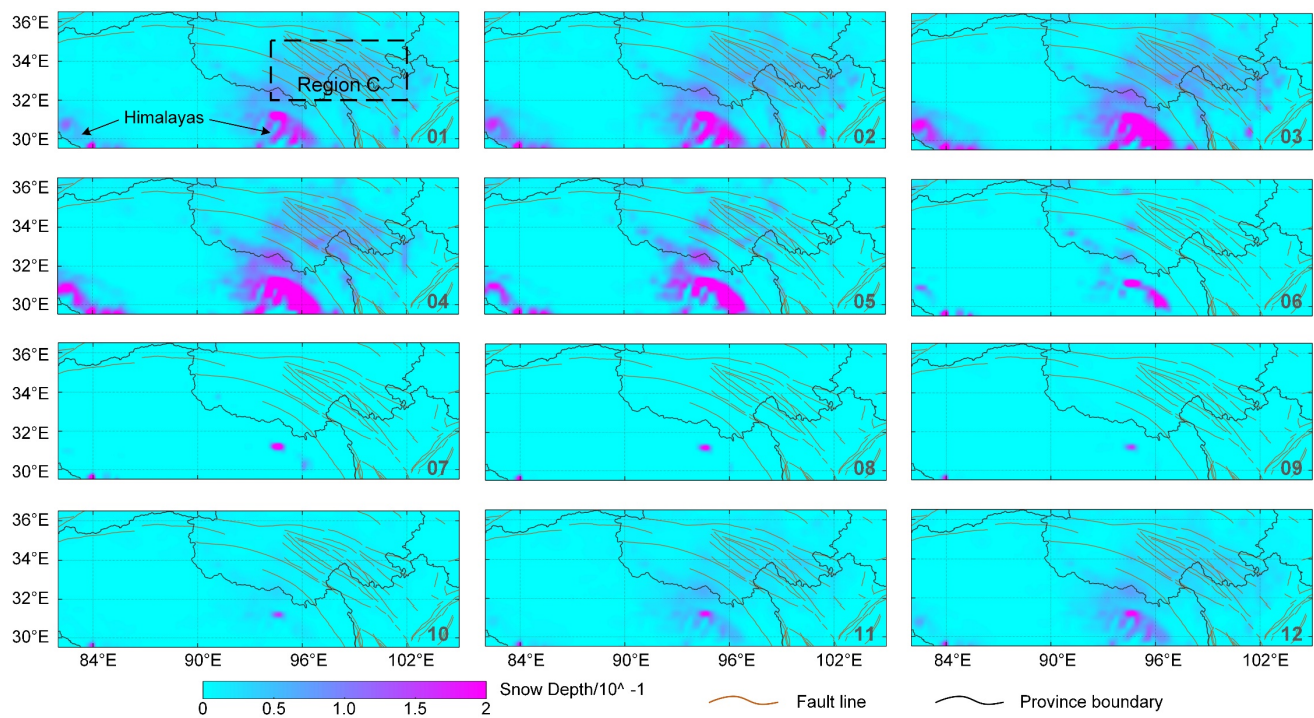


Figure 6. Monthly mean snow depth in the study area.

Snow depth represents the result of sustained snowfall in an area, and its monthly mean value represents its average over a month. Figure 6 indicates that the areas with large snow depth are mainly located in the permanent freeze area (Figure 1b), which belongs spatially to the central part and eastern end of the Himalayas (south part of the study area). In the border area of Tibet, Sichuan and Qinghai Provinces (region C), another area with small snow depth exists in the beginning and end of each year. The value of snow depth in region C increases from November to March, decreases from April to May and does not exist in the other months. The spatial distribution of snow depth in this area is in good agreement with that of the region with low SKT and high STD at high frequency. In Appendix A Figure A2, the values of STD at 89 GHz remain high from November to March, but the values of MBT at 89 GHz and SKT exhibit slight depressions relative to the overall annual trend in these months. These depressions are accompanied with high values of snow depth. Therefore, the aforementioned consistency in time and space indicates that the variation of snow depth due to snowfall events can disturb high-frequency MBT.

3.3. Application to Extract Seismic MBT Anomaly

The monthly mean MBT background reflects the usual state of microwave radiation emitted from the ground surface, and an abnormal MBT significantly exceeding the normal level accompanied with an EQ can be regarded as a seismic MBT anomaly. In practice, the dynamic monthly mean backgrounds of MBT need to be constructed according to the target date to be studied before and after the EQ (i.e., based on the data of 14 days before and 14 days after the target date) instead of directly using the average MBT of the current month. In this manner, the possible MBT anomaly can be effectively emphasised. The extraction of MBT anomaly is described in the following formulas:

$$MBT'_{\xi} = \frac{\sum_{\psi=\alpha}^{\psi=\beta} \sum_{\lambda=\xi-14}^{\lambda=\xi+14} MBT_{\psi,\lambda}}{\omega} \quad (2)$$

$$\Delta MBT_{\xi} = MBT_{\xi} - MBT'_{\xi} \quad (3)$$

where ζ represents the target day before, on or after the mainshock day. ψ and λ represent the year and day of available MBT data involved in the calculation, while α and β refer to the start and end years of available MBT data on day λ , ω stands for the total number of valid MBT data used for calculation. $MBT_{\psi,\lambda}$ is the available MBT data on year ψ and day λ . MBT'_{ζ} represents the dynamic monthly mean background of MBT for day ζ in the study area. MBT_{ζ} refers to original MBT data on day ζ , while ΔMBT_{ζ} is the obtained MBT anomaly possibly associated with EQ on day ζ .

In this study, the Ms 7.1 Yushu EQ on 13 April 2010 and the Ms 7.4 Maduo EQ on 21 May 2021, which are both strike-slip EQs that occurred within the Bayan Har block, were selected for a case study. According to CENC (<https://ceic.ac.cn> (accessed on 19 November 2021)), the Yushu EQ occurred on the south margin of the Bayan Har block, with its mainshock epicentre located at (33.17°N, 96.55°E) and with a hypocentre depth of 14 km. The Maduo EQ occurred near the north margin of the Bayan Har block, with its mainshock epicentre located at (34.65°N, 98.40°E) and with a hypocentre depth of 9 km.

Figure 7 shows the extracted residual MBT with 10.65 GHz at H-pol before, during and after the Yushu EQ on 13 April 2010. Overall, MBT anomalies were concentrated and significant in the short impending period (8 days) before the EQ, remained obvious within one week after the mainshock, then disappeared completely. In the February 2010, the study area remained calm and no significant abnormal phenomena were observed. Then, a slight abnormal stripe appeared to north of the epicenter on 2 March and a weak regional abnormal MBT appeared east near the epicenter on 28 March. On 5 April, a very typical strip-shaped positive MBT anomaly exactly covering the Bayan Har block occurred to north of the forthcoming epicenter (circled in red line). The amplitude of the anomalous MBT stripe was much larger than that before, and the scope of the stripe was right inside the massif (not completely covered). A week before the mainshock (on 6 April), a significant abnormal MBT was visible, but it seemed to move towards the east compared with that on 5 April (not absolutely due to data missing). A day before the mainshock, an obvious MBT anomaly occurred near the forthcoming epicenter and in the southwestern corner of the study area. On 13 April, the mainshock day, a large area with a positive MBT anomaly was observed around the epicenter, which lasted until 14 April, but the intensity was slightly lower than that of the typical strip-shaped anomaly that appeared on 5 April. A week after the mainshock (on 20 April), a significant positive MBT anomaly reoccurred around the epicenter, with its location and shape similar to those of the anomaly that occurred on the mainshock day. From the day before the mainshock to a week after the mainshock, the distribution of MBT anomalies was generally wide, but was basically around the epicenter. Afterwards, no significant positive MBT anomalies appeared and the study area returned to a state of calm in late April and May 2010. According to the analysis of the low-frequency MBT background, the typical abnormal stripe and the regional MBT anomalies around the epicenter did not present any spatial correlation with low frequency STD and SSM change; thus, they can be preliminarily identified as independent of the natural variations contained in the background.

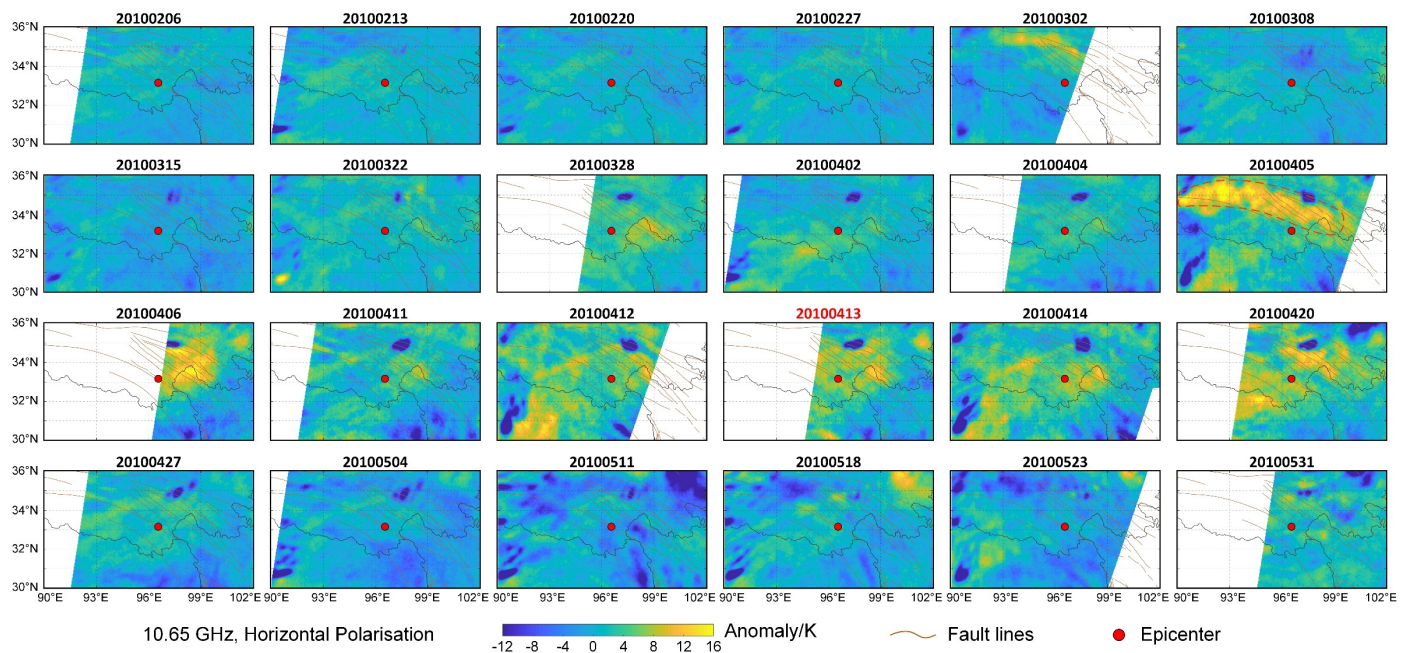


Figure 7. Spatio-temporal evolution of MBT anomalies with 10.65 GHz at H-pol related to the 2010 Yushu EQ.

Figure 8 presents the obtained *MBT* anomalies with 10.65 GHz at H-pol before, during and after the Maduo EQ on 21 May 2010. Overall, the *MBT* anomalies of the Maduo EQ were mainly concentrated in one and a half months before the mainshock, and the morphology of the anomalies was more complex, and different from that of the Yushu EQ in 2010. As early as the middle of January 2021, a positive *MBT* anomaly appeared in the south near the forthcoming epicenter inside the Bayan Har block. Then a regional anomaly appeared intermittently on 6 February and 25 February, with relatively small ranges and moderate intensities. As the March began, the positive *MBT* anomalies became much more prominent than before and emerged mainly as a large area around the epicenter, with its amplitude reaching the peak in mid and late March (one and a half month before the mainshock). The positive *MBT* anomalies were still obvious in early and middle April, but they showed a weakening trend in late April 2021. Two weeks before the mainshock, significant *MBT* anomalies appeared again around the upcoming epicenter, but with lower intensity than that in late March. Subsequently, the amplitude of the *MBT* anomalies showed a downward trend again until the EQ occurred on 21 May. After the mainshock day, the study area further showed a large area with negative values, and no significant positive *MBT* anomaly appeared in the same positions as before. To sum up, three kinds of positive *MBT* anomalies occurred from January to May before the Maduo EQ. The first was the regional anomaly around the epicenter, the second was the strip-shaped anomaly covering part of the Bayan Har block, and the third was the arc strip anomaly pointing from the southwest direction to the forthcoming epicenter. Additional detailed description and discussions of the three categories can be found in [55]. In particular, the abnormal *MBT* behaved as a prominent positive strip just covering part of the Bayan Har block on 9 March, 18 April and 19 April (circled in red line). Two weeks before the EQ, the *MBT* anomalies in the middle of the study area developed along the Bayan Har block, but their intensity was relatively low, and they did not behave so typically as they did before. With regard to the *MBT* background at 10.65 GHz, its usual variation was mainly contributed by SSM and SKT. However, the anomaly results obtained in this study were not well correlated with these critical parameters in spatial morphology. Therefore, the three categories of abnormal *MBT* can be preliminarily identified as seismic anomalies, but the mechanism and its relation to the EQ need further discussion.

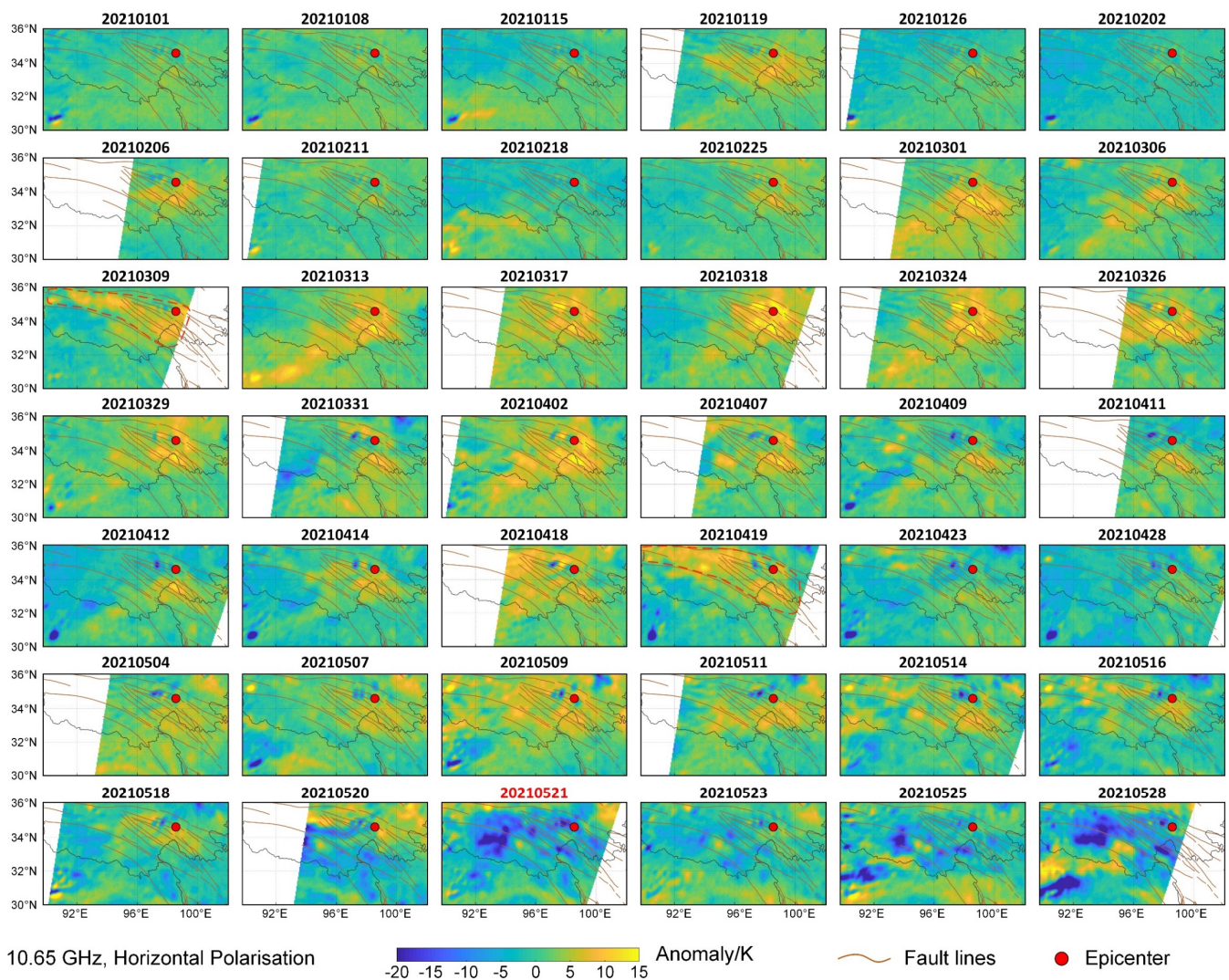


Figure 8. Spatio-temporal evolution of MBT anomalies with 10.65 GHz at H-pol related to the 2021 Maduo EQ.

4. Discussion

4.1. Discrimination of the MBT Anomalies

By referring to the dynamic monthly mean MBT background in the study area, a typical stripe of positive MBT anomalies covering part of the Bayan Har block was found prior to the Yushu EQ and the Maduo EQ. The authenticity of this special phenomenon and its potential causes deserves further discussion. For this purpose, the variation curves of averaged positive MBT anomalies before and after the two EQs inside the area of Bayan Har block were calculated. The synchronous change curves of averaged MBT, SKT, SSM and precipitation together with the two times STD of historical data for MBT, SKT in the same area were also obtained to analyze their trends and discuss their potential influences on the obtained MBT anomalies. The time series of the results are shown in Figure 9.

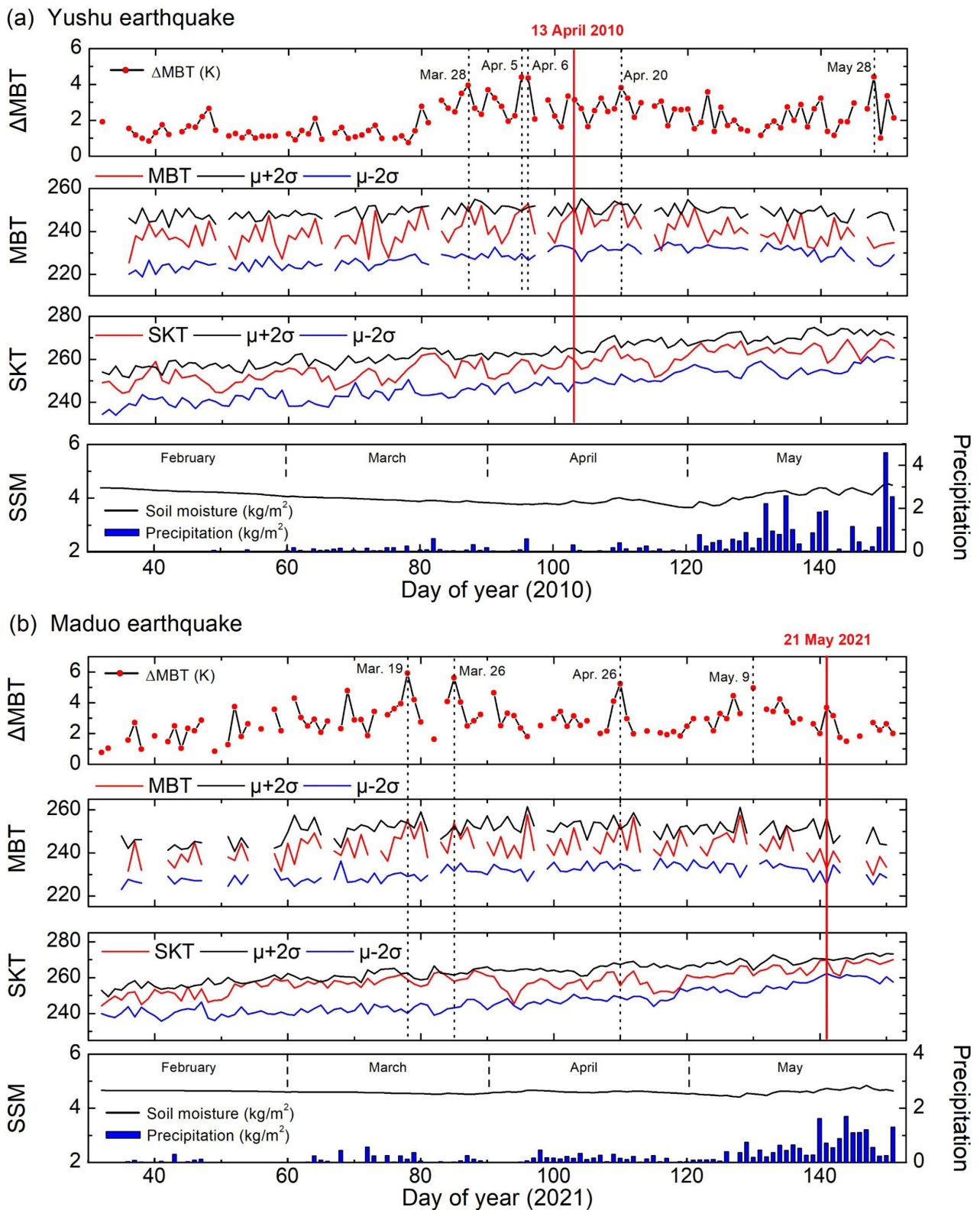


Figure 9. Variations of averaged MBT together with its anomalies, SKT, SSM, and precipitation within Bayan Har block before and after the Yushu EQ (a) and the Maduo EQ (b).

According to microwave remote sensing physics, the microwave radiation of the ground surface depends largely on surface temperature and microwave dielectric properties. In Figure 9, the curves of averaged MBT and SKT exhibited the multi-year stable state of microwave radiation and surface temperature within the Bayan Har block (μ), respectively.

And two times multi-year STD showed the volatility between same-day data over many years (σ). If the values of MBT and SKT fluctuated greatly in the EQ year, even beyond the range of multi-year mean value plus two times STD ($\mu + 2\sigma$), it can be regarded a potential anomaly. If SKT was in normal state when MBT exceeded the threshold ($\mu + 2\sigma$), the connection between the MBT anomaly and temperature can be excluded. The contribution of microwave emissivity change should be further explored, and then soil moisture change needs to be analyzed. After excluding the contributions of key non-seismic factors, the retained surface microwave radiation anomalies can be regarded as seismic-related.

With regard to the Yushu EQ (see Figure 9a), the curve of the MBT anomalies maintained low level without obvious mutation before March 2010. In late March and early April, the curve of the MBT anomaly went up dramatically, especially on 28 March, 5 April and 6 April. After the Yushu EQ, due to the rise of SSM caused by precipitation, MBT residuals in the study area showed an obvious depression, but several high values, such as those on 20 April and 28 May, still existed. The curves of the averaged MBT basically kept a fluctuating rising trend from February to April and then showed a slow downward trend in May, but the curves of averaged SKT only presented a roughly monotonous rise, reflecting the seasonal temperature changes. The inconsistency confirmed that the general change of MBT was not only affected by temperature, but also affected by microwave emissivity. On some critical dates, such as on 28 March, 5 April and 6 April, 2010, the magnitude of the MBT in the seismic year exceeded the threshold ($\mu + 2\sigma$), but the synchronous SKT was not so significant in these dates. This indicates that the change of MBT did not come from the contribution of SKT. Thus, the temperature was not the main reason for the seismic MBT anomalies. Furthermore, there were no significant changes in SSM at the time points corresponding to such significant positive abnormal MBT, which indicates that the impacts from soil moisture can be also excluded and the aforementioned abnormal phenomena may only be related to seismic activity. Concretely, the dramatically increase in MBT before 13 April 2010, such as on 28 March and 5 April, might be caused by the preparation of mainshock, while the slighter MBT anomalies after the Yushu EQ, such as on 20 April and 28 May, might be related to the large aftershocks on 20 April and 29 May, respectively (see Figure 10a).

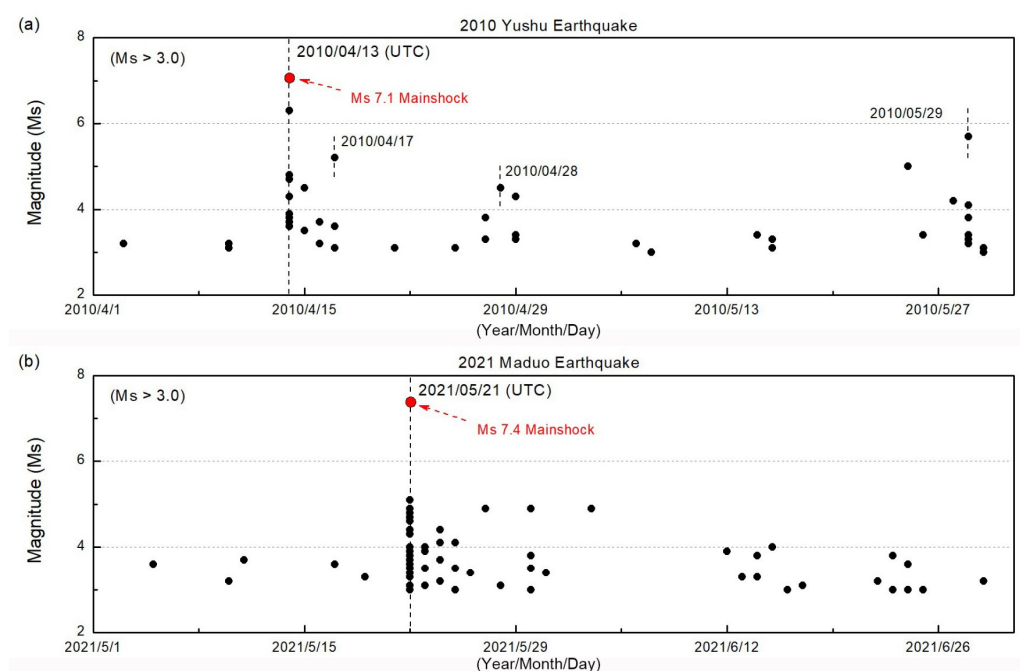


Figure 10. Diagrams of EQ frequency before, during, and after the 2010 Yushu EQ (a) and the 2021 Maduo EQ (b).

With regard to the Maduo EQ (see Figure 9b), the MBT anomaly remained very active throughout March and April 2021, with high values occurring much frequently, such as on 19 March, 26 March and 26 April. About ten days before the Maduo EQ, the MBT curve returned to high values, such as that on 9 May, despite the increased SSM and precipitation. From January to May 2021, the change trend of MBT and SKT was basically consistent with the Figure 9a, indicating that MBT was affected by multiple factors. On dates such as 19 March, 28 March and 26 April, these MBT anomalies correspond to MBT amplitude in seismic year exceeding the threshold ($\mu + 2\sigma$), while the synchronous SKT variation was normal. This also suggests that the significant MBT anomalies before the Maduo EQ did not contain obvious contributions of temperature. Similar to the situation in the Yushu EQ, the curves of SSM curve were mainly affected by rainfall and showed no significant correspondences with the change of the MBT. Hence, the retained significant MBT anomalies can be identified as closely related to the preparation phase of mainshock. However, in May and June 2021, the arrival of the rainy season on the plateau led to a sharp increase in local rainfall, swamping the supposed MBT anomalies around the epicenter shortly before and after the mainshock (aftershocks see Figure 10b).

On the basis of the above analysis, it is believed that the MBT anomalies inside the Bayan Har block before the 2010 Yushu EQ and the 2021 Maduo EQ were not caused by the changes in surface temperature or soil moisture. These MBT anomalies can be regarded to be caused by the EQs, and its geophysical and remote sensing physical mechanisms need to be further discussed.

4.2. Possible Causes of the Seismic MBT Anomalies

The 2010 Yushu EQ and 2021 Maduo EQ are strike-slip EQs that occurred on the Tibetan Plateau under the background of the Indian Ocean plate pressing against the Eurasian plate. The Yushu EQ happened in the Jinshajiang suture zone at the junction of the Qiangtang block and the Bayan Har block (Figure 1a). The seismogenic fault of the Yushu EQ was the Ganzi-Yushu fault on the southern boundary of the Bayan Har block, which is a left-lateral strike-slip fault strongly active in late Quaternary [56]. According to the GPS velocity field [57], the southern compression from the Indian plate turned significantly eastward after passing the Bayan Har block, suggesting that the northward movement of the massif was blocked by the Qaidam block in the north. The fault zone between the Bayan Har block and the Qaidam block was suitable for forming a compression stress concentration area, and the areas with the most significant eastward shift corresponded well to the location of MBT anomalies in early March 2010. This consistency indicates that the Bayan Har block had produced thermal anomalies due to local stress concentration. Half a month later, abnormal band-shaped TIR and OLR occurred along the Bayan Har block on 17 March 2010 [10,58], their shapes and locations were very similar to that of the MBT anomalies occurred on 5 April. Generally, the infrared thermal anomalies are mainly related to temperature changes and gas leakage, their appearance heralded that micro-fracture in the crustal rock has occurred in large numbers. The phenomenon reflected that the surface thermal response of crust stress in this period tended to present as a strip along the Bayan Har block. Numerical simulation of equivalent stress variation caused by 2010 Yushu EQ exhibited similar spatial distribution to these thermal anomalies within the block [59], which proved that the long-term stress accumulation and release pattern of Yushu EQ was indeed along the Bayan Har block. In late March and early April 2010, the TIR and OLR anomalies occurred as strips roughly perpendicular to the faults [60,61], their spatial patterns were consistent with the MBT anomalies widely distributed shortly before and after Yushu EQ (i.e., from 12 April to 20 April). This phenomenon implies that the influence of crust stress variation before and after the Yushu EQ was further expanded.

The Maduo EQ occurred near the east Kunlun fault on the north margin of the Bayan Har block, and the seismogenic fault was identified as the Maduo-Gande fault (Figure 1a), which is also a sinistral strike-slip fault active in Holocene [62]. The focal mechanisms of the Maduo EQ and the Yushu EQ were similar, but the occurrences of

significant MBT anomalies before the Maduo EQ were much earlier. In mid-January and early February 2021, the intermittent appearance of the MBT anomalies around the future epicenter indicated that the crust stress state was in a state of drastic adjustment and might enter a state of rapid aggregation in March, resulting in the concentration of MBT anomalies with large amplitudes during this time (such as 24 March and 26 March). Recent study reported that the temperature of well water in the Bayan Har block (about 220 km from the epicenter) dropped sharply in mid-March 2021 and then returned to normal state gradually. The mixing of the groundwater caused by crust rock fracturing was regarded as the cause after excluding the interference from instruments, human activities and the natural environment [63]. The synchronicity between changes in well water and MBT suggests that the block tectonics around the forthcoming hypocenter might have become very active during this period. About a month before the mainshock, the regional load/unload response ratio was revealed to vary greatly [47], which confirmed the dramatic variation of crustal stress. Therefore, the strip-shaped MBT anomalies covering part of the Bayan Har block on 18 April and 19 April seemed to be reasonable. In late April and May, the arrival of rainy season on the plateau greatly reduced the surface microwave radiation and shielded seismic thermal anomalies. In spite of this, there were still a small range of positive MBT anomalies in the central region of Bayan Har block, which indicates that the response of crust stress changes was so severe that the MBT anomalies were not drown completely shortly before the Maduo EQ. After the EQ, the soil moisture near the epicenter further increased, and there were no MBT anomalies similar to those before the Maduo EQ.

In our recent studies [36], a chain reaction has been proposed for interpreting seismic MBT anomalies, by integrating the knowledge of microwave remote sensing physics and P-holes theory [64]. The key point of this chain reaction is that the crustal stress variation causes positive charges to be generated from the crustal rock mass, and then diffused along stress gradient to concentrated selectively on the ground, thus changing the microwave dielectric of the shallow surface and causing microwave radiation anomalies. Through the analysis and discussion, many indirect information of crustal stress changes before, during and after the occurrences of the significant MBT anomalies were found. The stress concentration at deep crust could stimulate the generation, transmission and aggregation of positive charges, but it was affected by the location, rock mass medium and landcovers, so the stress responses occurred on the ground may migrate in different stages of seismogenic period. The Bayan Har block is densely faulted, and micro-cracks were easier to be generated due to stress accumulation than those outside the block, thus making the generation and transfer of positive charges inclined to interior. When positive charges reached the ground surface of the Bayan Har block, additional electric fields were generated instantaneously to alter the microwave dielectric properties and thus cause satellite-observed MBT anomalies.

With regard to the differences between the MBT anomalies of the two EQ cases, the seismogenic mechanisms should be considered. The Yushu EQ was a foreshock—mainshock—aftershock type, with one strong aftershock of $M_s > 6.0$ and several aftershocks of $M_s > 5.0$, the energy accumulated during the seismogenic period of the Yushu EQ was not fully released by the mainshock, which might have led to the moderate MBT anomalies after the mainshock (such as on 20 April). Meanwhile, the aftershocks of the Maduo EQ were lower in magnitude, and the plateau area was highly affected by the heavy rainfall after May. Thus no obvious post-earthquake MBT anomalies occurred. Furthermore, the Yushu EQ had a lower magnitude and a deeper hypocenter depth compared to the Maduo EQ, signals from deep crustal stress changes had greater loss on the way of transmission to ground surface. Therefore, the MBT anomalies before the Yushu EQ could be smaller in scope and lower in amplitude than those before the Maduo EQ.

5. Conclusions and Outlook

The research on seismic MBT anomalies and precursors is crucial for monitoring and providing a prewarning for large EQs. However, ideal and reliable precursors are difficult

to obtain because of the complexity and heterogeneity of the seismogenic environment. Focusing on the seismically active Bayan Har block on the Qinghai–Tibet Plateau, this research analysed the characteristics of the usual state of microwave radiation variation by using the monthly mean background of MBT. The aim is to provide a background reference for the study of abnormal MBT possibly related to seismicity and EQs.

The obtained monthly mean H-polarised MBT backgrounds at 10.65 and 89 GHz presented obvious negative correlations with altitude. This correlation was significant in each month and became increasingly significant for the MBT residuals at high frequency. In the plateau area with a high altitude, the MBT background at 10.65 GHz showed a complex trend of increasing from January to May, decreasing from May to August, increasing again from August to October and decreasing from October to December. This complex process was determined to be jointly affected by SSM and seasonal temperature. The MBT background at 89 GHz showed a trend of rising from spring to summer then falling from autumn to winter, which was consistent with the variation of seasonal atmospheric temperature. In the mountain area with a relatively low altitude, the MBT backgrounds at the two frequencies exhibited good agreement with the variation of surface temperature. Moreover, the monthly standard deviation of MBT at the two frequencies was calculated. By using auxiliary data, the high values of the monthly standard deviation of MBT at low frequency were determined to be caused by SSM variation, whereas those at high frequency were proven to be affected by snowfall events.

On the basis of the dynamic monthly mean MBT background, significant MBT anomalies at 10.65 GHz associated with the 2010 Ms 7.1 Yushu EQ and 2021 Ms 7.4 Maduo EQ were revealed. Very prominent positive MBT anomalies were found appearing around the epicenter and along the active faults before, during and after the two EQs. A typical strip-shaped positive MBT anomaly covering exactly the Bayan Har block preceded the two mainshocks, and was regarded as a precursor with certain commonness. The variation of the average MBT anomalies inside the Bayan Har block was analyzed and discriminated by using multiple datasets, and then was discussed referring to existing theories and case studies.

This study concentrated on the seismically active Bayan Har block, and the results demonstrated the necessity to establish the MBT background field for the study area before analysing seismic MBT anomalies. The methodology and ideas presented here are not only instructive for monitoring seismic activity and potential large EQs on the Qinghai–Tibet Plateau, but also valuable to other seismically active regions, such as the Longmenshan fault zone in Sichuan, China, the Himalayan nappe zone and the Iran–Iraq border area. Prior knowledge of MBT background information is helpful in searching for seismic MBT anomalies from complex microwave radiation information that contains geographical differences, landcover differences and meteorological disturbances.

Author Contributions: Conceptualization, Y.Q.; Data curation, Y.D., Y.L. and X.W.; Formal analysis and concept recognition, L.W. and W.M.; Funding acquisition, L.W.; Methodology, Y.Q.; Validation, Y.D., Y.L. and W.M.; Visualization, Y.D. and Y.L.; Writing—original draft, Y.Q.; Writing—review & editing, Y.Q. and L.W. All authors have read and agreed to the published version of the manuscript.

Funding: This research was funded by the National Key R & D Program of China, grant number 2018YFC15035, the Key Program of the National Natural Science Foundation of China, grant number 41930108, the innovation leading program of Central South University, grant number 506030101, and the Talents Gathering Program of Hunan Province, China, grant number 2018RS3013.

Data Availability Statement: MBT data. Available online: <https://disc.gsfc.nasa.gov/datasets> (accessed on 9 July 2021); Skin temperature and 2m air temperature data. Available online: <https://cds.climate.copernicus.eu/> (accessed on 21 November 2021); Soil moisture data and precipitation data. Available online: <https://earthdata.nasa.gov> (accessed on 27 July 2021).

Acknowledgments: MBT data, soil moisture and precipitation data were acquired and owned by NASA's Earth Observing System Data and Information System. Skin temperature and 2 m air temperature data were acquired and owned by Copernicus Climate Change Service.

Conflicts of Interest: The authors declare no conflict of interest.

Appendix A

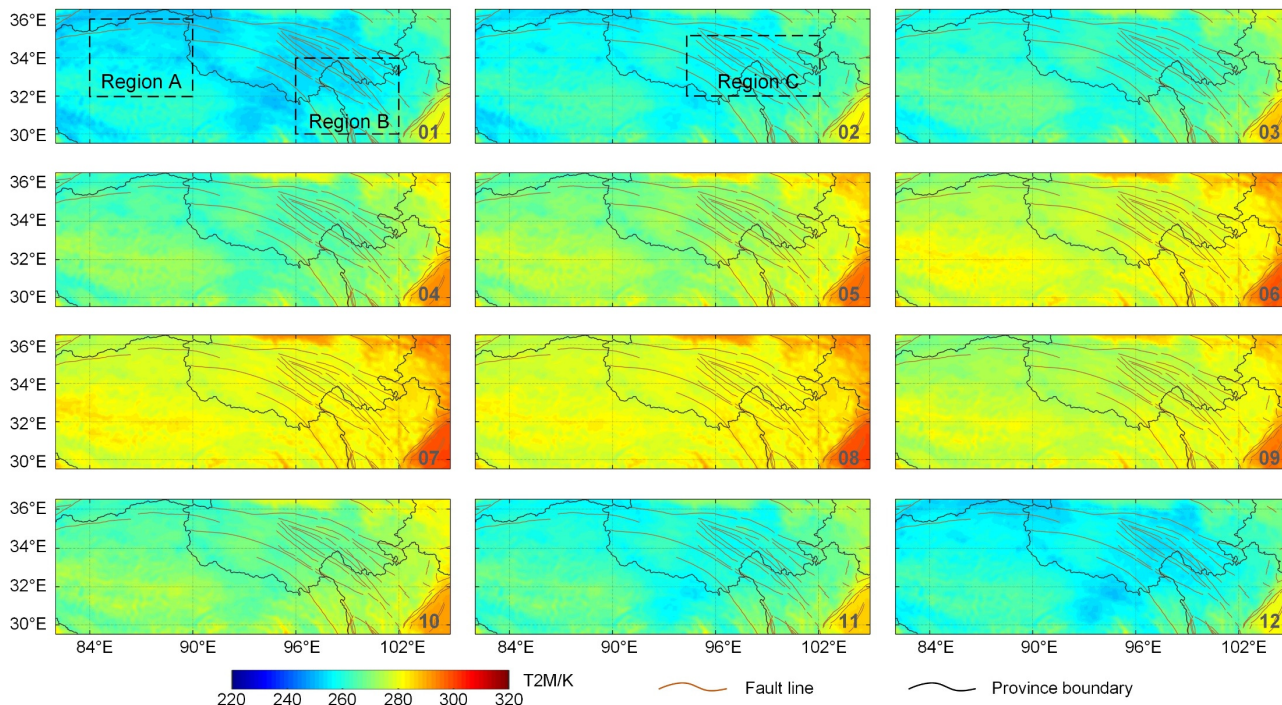


Figure A1. Monthly mean T2M in the study area.

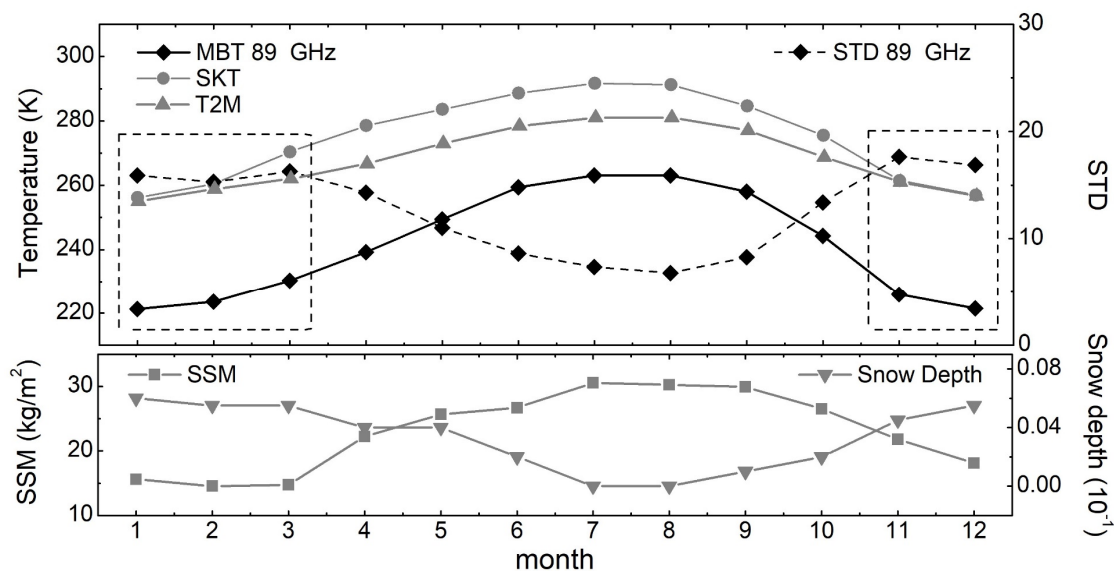


Figure A2. Variations of MBT background and STD at 89 GHz, SKT, T2M, SSM and snow depth in region C.

References

- Gornyi, V.I.; Sal'Man, A.G.; Tronin, A.A.; Shilin, B.V. Outgoing infrared radiation of the earth as an indicator of seismic activity. *Akad. Nauk SSSR Dokl.* **1988**, *301*, 67–69.
- Wright, T.J.; Parsons, B.E.; Lu, Z. Toward mapping surface deformation in three dimensions using InSAR. *Geophys. Res. Lett.* **2004**, *31*, L01607. [[CrossRef](#)]
- Saraf, A.A.; Choudhury, S. Satellite detects surface thermal anomalies associated with the Algerian earthquakes of May 2003. *Int. J. Remote Sens.* **2004**, *26*, 2705–2713. [[CrossRef](#)]

4. Hayakawa, M.; Hattori, K.; Ohta, K. Monitoring of ULF (ultra-low-frequency) geomagnetic variations associated with earthquakes. *Sensors* **2007**, *7*, 1108–1122. [[CrossRef](#)]
5. Brunner, D.; Lemoine, G.; Bruzzone, L. Earthquake damage assessment of buildings using VHR optical and SAR imagery. *IEEE Trans. Geosci. Remote Sens.* **2010**, *48*, 2403–2420. [[CrossRef](#)]
6. Wu, L.X.; Qin, K.; Liu, S.J. GEOS- based thermal parameters analysis for earthquake anomaly recognition. *Proc. IEEE* **2012**, *100*, 2891–2907. [[CrossRef](#)]
7. Dell’Acqua, F.; Gamba, P. Remote sensing and earthquake damage assessment: Experiences, limits, and perspectives. *Proc. IEEE* **2012**, *100*, 2876–2890. [[CrossRef](#)]
8. Liu, S.J.; Liu, X.; Ma, Y.T.; Wu, L.X. Microwave radiation anomaly of Yushu earthquake and its mechanism. In Proceedings of the 2011 IEEE International Geoscience and Remote Sensing Symposium, Vancouver, BC, Canada, 24–29 July 2011; IEEE: New York, NY, USA, 2011; pp. 1192–1195. [[CrossRef](#)]
9. Liu, W.; Yamazaki, F. Extraction of collapsed bridges due to the 2011 Tohoku-oki earthquake from post-event SAR images. *J. Disaster. Res.* **2018**, *13*, 281–290. [[CrossRef](#)]
10. Qin, K.; Wu, L.X.; Zheng, S.; Ma, W.Y. Discriminating satellite IR anomalies associated with the MS 7.1 Yushu earthquake in China. *Adv. Space. Res.* **2018**, *61*, 1324–1331. [[CrossRef](#)]
11. Ouzounov, D.; Pulinets, S.; Hattori, K.; Taylor, P. *Pre-Earthquake Processes: A Multidisciplinary Approach to Earthquake Prediction Studies*, 3rd ed.; John Wiley & Sons, Inc: Hoboken, NJ, USA, 2018. [[CrossRef](#)]
12. Zhang, Y.; Meng, Q.Y.; Ouillon, G.; Sornette, D.; Ma, W.Y.; Zhang, L.L.; Zhao, J.; Qi, Y.; Geng, F. Spatially variable model for extracting TIR anomalies before earthquakes: Application to Chinese Mainland. *Remote Sens. Environ.* **2021**, *267*, 112720. [[CrossRef](#)]
13. Qi, Y.; Wu, L.X.; Ding, Y.F.; Mao, W.F. Microwave brightness temperature anomalies associated with the 2015 Mw 7.8 Gorkha and Mw 7.3 Dolakha earthquakes in Nepal. *IEEE Trans. Geosci. Remote Sens.* **2022**, *60*, 1–11. [[CrossRef](#)]
14. Qi, Y.; Miao, Z.L.; Wu, L.X.; Ding, Y.F. Seismic microwave brightness temperature anomaly detection using multitemporal passive microwave satellite images: Ideas and limits. *IEEE J. Sel. Top. Appl. Earth Obs. Remote Sens.* **2021**, *14*, 6792–6806. [[CrossRef](#)]
15. Ulaby, F.T.; Moore, R.K.; Fung, A.K. *Microwave Remote Sensing Fundamentals and Radiometry*. In *Microwave Remote Sensing Active and Passive*, 2nd ed.; Addison-Wesley: Boston, MA, USA, 1981.
16. Ulaby, F.T.; David, L. *Microwave Radar and Radiometric Remote Sensing*, 3rd ed.; The University of Michigan Press: Ann Arbor, MI, USA, 2014.
17. Curtis, J.O. Moisture effects on the dielectric properties of soils. *IEEE Trans. Geosci. Remote Sens.* **2001**, *39*, 125–128. [[CrossRef](#)]
18. Turner, D.D.; Clough, S.A.; Liljegren, J.C.; Clothiaux, E.E.; Cady-Pereira, K.E.; Gaustad, K.L. Retrieving liquid water path and precipitable water vapor from the atmospheric radiation measurement (ARM) microwave radiometers. *IEEE Trans. Geosci. Remote Sens.* **2007**, *45*, 3680–3690. [[CrossRef](#)]
19. Bauer, P.; Schuessel, P. Rainfall, total water, ice water, and water vapor over sea from polarized microwave simulations and special sensor microwave/imager data. *J. Geophys. Res. Atmos.* **1993**, *98*, 20737–20759. [[CrossRef](#)]
20. Njoku, E.G.; Jackson, T.J.; Lakshmi, V.; Chan, T.K.; Nghiem, S.V. Soil moisture retrieval from AMSR-E. *IEEE Trans. Geosci. Remote Sens.* **2003**, *41*, 215–229. [[CrossRef](#)]
21. Njoku, E.G.; Entekhabi, D. Passive microwave remote sensing of soil moisture. *J. Hydrol.* **1996**, *184*, 101–129. [[CrossRef](#)]
22. Karbou, F.; Gérard, É.; Rabier, F. Microwave land emissivity and skin temperature for AMSU-A and -B assimilation over land. *Q. J. R. Meteor. Soc.* **2006**, *132*, 2333–2355. [[CrossRef](#)]
23. Li, Z.L.; Tang, B.H.; Wu, H.; Ren, H.Z.; Yan, G.J.; Wan, Z.M.; Trigo, I.F.; Sobrino, J.A. Satellite-derived land surface temperature: Current status and perspectives. *Remote Sens. Environ.* **2013**, *131*, 14–37. [[CrossRef](#)]
24. Kelly, R.E.; Chang, A.T.; Tsang, L.; Foster, J.L. A prototype AMSR-E global snow area and snow depth algorithm. *IEEE Trans. Geosci. Remote Sens.* **2003**, *41*, 230–242. [[CrossRef](#)]
25. Pulliainen, J. Mapping of snow water equivalent and snow depth in boreal and sub-arctic zones by assimilating space-borne microwave radiometer data and ground-based observations. *Remote Sens. Environ.* **2006**, *101*, 257–269. [[CrossRef](#)]
26. Prigent, C.; Rossow, W.B.; Matthews, E. Microwave land surface emissivities estimated from SSM/I observations. *J. Geophys. Res. Atmos.* **1997**, *102*, 21867–21890. [[CrossRef](#)]
27. Prigent, C.; Rossow, W.B.; Matthews, E. Global maps of microwave land surface emissivities: Potential for land surface characterization. *Radio Sci.* **1998**, *33*, 745–751. [[CrossRef](#)]
28. Saraf, A.K.; Choudhury, S. Thermal remote sensing technique in the study of pre-earthquake thermal anomalies. *J. Ind. Geophys. Union* **2005**, *9*, 197–207. [[CrossRef](#)]
29. Takano, T.; Maeda, T. Experiment and theoretical study of earthquake detection capability by means of microwave passive sensors on a satellite. *IEEE. Geosci. Remote Sens. Lett.* **2009**, *6*, 107–111. [[CrossRef](#)]
30. Singh, R.P.; Zlotnicki, J.; Prasad, A.K.; Gautam, R.; Kafatos, M. Precursory signals using satellite and ground data associated with the Wenchuan earthquake of 12 May 2008. *Int. J. Remote Sens.* **2010**, *31*, 3341–3354. [[CrossRef](#)]
31. Maeda, T.; Takano, T. Detection algorithm of earthquake-related rock failures from satellite-borne microwave radiometer data. *IEEE Trans. Geosci. Remote Sens.* **2010**, *48*, 1768–1776. [[CrossRef](#)]
32. Chen, H.; Jin, Y.Q. A preliminary detection of anomalous radiation of rock failures related with Yushu earthquake by using satellite-borne microwave radiometers. *Remote Sens. Technol. Appl.* **2010**, *25*, 860–866. [[CrossRef](#)]

33. Ma, Y.T.; Liu, S.J.; Wu, L.X.; Xu, Z.Y. Two-step method to extract seismic microwave radiation anomaly: Case study of Ms 8.0 Wenchuan earthquake. *Earthq. Sci.* **2011**, *24*, 577–582. [[CrossRef](#)]
34. Jing, F.; Singh, R.P.; Sun, K.; Shen, X. Passive microwave response associated with two main earthquakes in Tibetan Plateau, China. *Adv. Space Res.* **2018**, *62*, 1675–1689. [[CrossRef](#)]
35. Qi, Y.; Wu, L.X.; He, M.; Mao, W.F. Spatio-temporally weighted two-step method for retrieving seismic MBT anomaly: May 2008 Wenchuan earthquake sequence being a case. *IEEE J. Sel. Top. Appl. Earth Obs. Remote Sens.* **2020**, *13*, 382–391. [[CrossRef](#)]
36. Qi, Y.; Wu, L.X.; Mao, W.F.; Ding, Y.F.; He, M. Discriminating possible causes of microwave brightness temperature positive anomalies related with May 2008 Wenchuan earthquake sequence. *IEEE Trans. Geosci. Remote Sens.* **2021**, *59*, 1903–1916. [[CrossRef](#)]
37. Ding, Y.F.; Qi, Y.; Wu, L.X.; Mao, W.F.; Liu, Y.J. Discriminating the multi-frequency microwave brightness temperature anomalies relating to 2017 Mw 7.3 Sarpol Zahab (Iran-Iraq border) earthquake. *Front. Earth Sci.* **2021**, *706*, 656216. [[CrossRef](#)]
38. Qi, Y.; Wu, L.X.; Mao, W.F.; Ding, Y.F.; Liu, Y.J. Satellite Passive Microwave Remote Sensing for Seismic Thermal Anomaly: Phenomena and Mechanisms. In Proceedings of the 2021 IEEE International Geoscience and Remote Sensing Symposium, Brussels, Belgium, 11–16 July 2021; IEEE: New York, NY, USA; pp. 8696–8699. [[CrossRef](#)]
39. Liu, S.J.; Xu, Z.Y.; Wei, J.L.; Huang, J.W.; Wu, L.X. Experimental study on microwave radiation from deforming and fracturing rock under loading outdoor. *IEEE Trans. Geosci. Remote Sens.* **2016**, *54*, 5578–5587. [[CrossRef](#)]
40. Gao, X.; Liu, S.J.; Wu, L.X.; Mao, W.F.; Li, W.W.; Huang, J.W. The variation in microwave brightness temperature of granite pressed under weak background radiation. *IEEE Trans. Geosci. Remote Sens.* **2020**, *59*, 1369–1381. [[CrossRef](#)]
41. Gao, X.; Liu, S.J.; Wu, L.X.; Mao, W.F.; Li, W.W.; Huang, J.W.; Mao, W.F. The anisotropy and polarization of stress-induced microwave radiation changes in granite and their significance for seismic remote sensing. *IEEE Trans. Geosci. Remote Sens.* **2021**, *59*, 7603–7617. [[CrossRef](#)]
42. Mao, W.F.; Wu, L.X.; Liu, S.J.; Gao, X.; Huang, J.W.; Xu, Z.Y.; Qi, Y. Additional microwave radiation from experimentally loaded granite covered with sand layers: Features and mechanisms. *IEEE Trans. Geosci. Remote Sens.* **2020**, *58*, 5008–5022. [[CrossRef](#)]
43. Mao, W.F.; Wu, L.X.; Qi, Y. Impact of compressive stress on microwave dielectric properties of feldspar specimen. *IEEE Trans. Geosci. Remote Sens.* **2020**, *58*, 1398–1408. [[CrossRef](#)]
44. Zoran, M. MODIS and NOAA-AVHRR I and surface temperature data detect a thermal anomaly preceding the 11 March 2011 Tohoku earthquake. *Int. J. Remote Sens.* **2012**, *33*, 6805–6817. [[CrossRef](#)]
45. Deng, Q.D.; Gao, X.; Chen, G.H.; Yang, H. Recent tectonic activity of Bayankala fault block and the Kunlun Wenchuan earthquake series of the Tibetan Plateau. *Earth Sci. Front.* **2010**, *17*, 163.
46. Woerd, J.V.D.; Tapponnier, P.; Ryerson, F.J.; Meriaux, A.S.; Meyer, B.; Gaudemer, Y.; Finkel, R.C.; Caffee, M.W.; Zhao, G.G.; Xu, Z.Q. Uniform postglacial slip-rate along the central 600 km of the Kunlun Fault (Tibet), from ²⁶Al, ¹⁰Be, and ¹⁴C dating of riser offsets, and climatic origin of the regional morphology. *Geophys. J. Int.* **2002**, *148*, 356–388. [[CrossRef](#)]
47. Wang, S.Y.; Tian, H.; Ma, K.X.; Yu, C.; Ma, W.Y.; Yu, H.Z. Correlation between short-term and imminent anomalies of LURR and OLR before the Maduo Ms7.4 earthquake in Qinghai Province. *China Earthq. Eng. J.* **2021**, *43*, 847–852, 859. [[CrossRef](#)]
48. Liu, J.; Du, X.B.; Jacques, Z.; Fan, Y.Y.; An, Z.H.; Xie, T.; Zheng, G.L.; Tan, D.C.; Chen, J.Y. The changes of the ground and ionosphere electric/magnetic fields before several great earthquakes. *Chin. J. Geophys.* **2011**, *54*, 2885–2897. [[CrossRef](#)]
49. Zhao, S.F.; Shen, X.H.; Zhima, Z.; Zhou, C. The very low-frequency transmitter radio wave anomalies related to the 2010 Ms 7.1 Yushu earthquake observed by the DEMETER satellite and the possible mechanism. *Ann. Geophys.* **2020**, *38*, 969–981. [[CrossRef](#)]
50. Dong, C.; Chen, B.; Yuan, J.C.; Wang, Z.D.; Wang, C. Characteristic analysis of the lithospheric magnetic anomaly before the Madoi M S 7.4 earthquake on 22th May 2021. *Acta Seismol. Sin.* **2021**, *43*, 453–462. [[CrossRef](#)]
51. Prigent, C.; Aires, F.; Rossow, W.B. Land surface microwave emissivities over the globe for a decade. *Bull. Am. Meteorol. Soc.* **2006**, *87*, 1573–1584. [[CrossRef](#)]
52. Prigent, C.; Aires, F.; Rossow, W.; Matthews, E. Joint characterization of vegetation by satellite observations from visible to microwave wavelengths: A sensitivity analysis. *J. Geophys. Res. Atmos.* **2001**, *106*, 20665–20685. [[CrossRef](#)]
53. Weng, F.Z.; Yan, B.H.; Grody, N.C. A microwave land emissivity model. *J. Geophys. Res. Atmos.* **2001**, *106*, 20115–20123. [[CrossRef](#)]
54. Jackson, T.J., III. Measuring surface soil moisture using passive microwave remote sensing. *Hydrol. Process.* **1993**, *7*, 139–152. [[CrossRef](#)]
55. Qi, Y.; Wu, L.; Ding, Y.; Liu, Y.; Chen, S.; Wang, X.; Mao, W. Extraction and discrimination of MBT anomalies possibly associated with the Mw 7.3 Maduo (Qinghai, China) Earthquake on 21 May 2021. *Remote Sens.* **2021**, *13*, 4726. [[CrossRef](#)]
56. Institute of Geology, China Seismological Bureau. Analysis of Source Area Seismotectonics of Yushu Ms 7.1 Earthquake. 2010. Available online: <http://www.eq-igl.ac.cn> (accessed on 19 November 2021).
57. Gan, W.J.; Zhang, P.Z.; Shen, Z.K.; Niu, Z.J.; Wang, M.; Wan, Y.G.; Zhou, D.M.; Cheng, J. Present-day crustal motion within the Tibetan Plateau inferred from GPS measurements. *J. Geophys. Res. Solid Earth* **2007**, *112*, B08416. [[CrossRef](#)]
58. Qin, K.; Wu, L.X.; Zheng, S.; Liu, S.J. A deviation-time-space-thermal (DTS-T) method for global earth observation system of systems (GEOSS)-based earthquake anomaly recognition: Criteria and quantify indices. *Remote Sens.* **2013**, *5*, 5143–5151. [[CrossRef](#)]
59. Yang, X.Y.; Yang, L.M.; Li, Y.J.; Tan, P. Numerical simulation on strong earthquake dynamic process of Bayan Har block. *Acta Seismol. Sin.* **2013**, *35*, 304–314. [[CrossRef](#)]
60. Wei, C.X.; Zhang, Y.S.; Xiao, G.; Qin, M.Z.; Ning, Y.L.; Gao, J. Thermal infrared and long-wave radiation anomalies of Yushu M_S7.1 earthquake. *Pro. In. Geophys.* **2013**, *28*, 2444–2452. [[CrossRef](#)]

61. Xie, T.; Kang, C.L.; Ma, W.Y. Thermal infrared brightness temperature anomalies associated with the Yushu (China) Ms = 7.1 earthquake on 14 April 2010. *Nat. Hazards Earth Syst. Sci.* **2013**, *13*, 1105–1111. [[CrossRef](#)]
62. Zhan, Y.; Liang, M.J.; Sun, X.Y.; Huang, F.P.; Zhao, L.Q.; Gong, Y.; Han, J.; Li, C.X.; Zhang, P.Z.; Zhang, H.P. Deep structure and seismogenic pattern of the 2021.5.22 Madoi (Qinghai) Ms7.4 earthquake. *Chin. J. Geophys.* **2021**, *64*, 2232–2252.
63. Su, W.G.; Liu, L.; Yuan, F.Q.; Zhao, Y.H.; Sun, X.H. The anomaly characteristics of well water temperature in Yushu seismic station before the 2021 Maduo MS7.4 earthquake. *Acta Geol. Sin.* **2021**, *43*, 1–5.
64. Freund, F. Toward a unified solid state theory for pre-earthquake signals. *Acta Geophys.* **2010**, *58*, 719–766. [[CrossRef](#)]